

Lattice Gas with Monte Carlo collision operator recovers lattice Boltzmann method

Thomas Blommel* and Alexander J. Wagner†

Department of Physics, North Dakota State University, Fargo, North Dakota 58108, USA

(Dated: March 25, 2019)

We are examining a new kind of lattice gas that closely resembles modern lattice Boltzmann methods. This new kind of lattice gas, that we call a Monte Carlo Lattice Gas, has interesting properties that shed light on the origin of the multi-relaxation time collision operator and it derives an equilibrium distribution that agrees to lowest order with the standard lattice Boltzmann equilibrium distribution. Furthermore these lattice gas methods have natural fluctuations, giving further insight into the properties that we should expect for fluctuating lattice Boltzmann methods.

I. INTRODUCTION

Fluctuations originate because of nature is build out of discrete particles[1]. When one examines a small enough systems, these fluctuations, originating from the stochastic nature of the dynamics of the discrete particles, manifest themselves. With few exceptions, *e.g.* the dynamics close to a critical point[2], these fluctuations become irrelevant for larger systems, and the dynamics of this large-scale system becomes deterministic, allowing us to describe the system as a continuum. These continuum equations, like the continuity and Navier-Stokes equations for fluids, are enormously successful at describing macroscopic phenomena. So it is tempting to continue to utilize these continuous equations of motions down to scales where fluctuations become important. In these cases fluctuations, that were eliminated, have to be somehow re-introduced. One way to consistently introduce fluctuations is the Langevin approach[3], which consists of introducing a fluctuating term in the equations of motion and then adjusting the amplitude of the fluctuating term to give correct fluctuations in equilibrium. This is easily done since it is known that the states of the system obey a Boltzmann statistics.

This general narrative is the template for the development of fluctuating lattice Boltzmann methods. The original lattice gases introduced by Frisch, Hasslacher and Pomeau [4] consisted of a hexagonal lattice and particles moving along the links between nearest neighbor sites. The model was restricted to having at most one particle moving along each link. While it could be shown that this model had enough symmetry to recover the Navier-Stokes equations in the hydrodynamic limit, the model contained very large fluctuations, that needed to be averaged out to examine hydrodynamic phenomena. Part of the derivation of the Navier-Stokes equations required taking a formal ensemble average of the lattice gas, leading to a Boltzmann equation for the lattice gas[5]. Mc Namara [6] then realized that one could use this Boltzmann averaged lattice gas as a method in its own right. This method became known as the lattice Boltzmann

method. The original lattice Boltzmann method was an exact ensemble average of the lattice gas, retaining the unconditional stability of the lattice gas as well as several of its flaws. At the time a key advantage of the new lattice Boltzmann method was the elimination of all noise.

Soon it was discovered that the lattice Boltzmann method could be simplified by using a BGK approximation for the collision operator [7]. The idea here is that the distribution function will approach the local equilibrium distribution, consistent with the locally conserved density and momentum. This significantly simplified the collision operation and at the same time removed some undesirable artifacts that had survived the transition from the lattice gas to the lattice Boltzmann methods, like the velocity dependence of the viscosity[5]. While the improvements of these novel lattice Boltzmann methods made them extremely popular any application that needed fluctuations was stuck with lattice gas methods. Tony Ladd had utilized the fluctuations of lattice gases to simulate the Brownian motion of colloids [8]. He then developed a fluctuating version of the lattice Boltzmann method by including a fluctuating stress tensor that would recover the fluctuating hydrodynamic equations [9]. While this recovered the correct hydrodynamic limit, the fluctuations could be seen to be only correct for wavelength of the size of the system. Other fluctuations were suppressed. The reason for this became clear when Adhikari *et al.* noticed that all kinetic modes, not only those related to the hydrodynamic quantities, needed to have fluctuations added[10]. The theoretical framework for this was work on generating a fluctuating version of the linearized Boltzmann equation by Bison and Zwanzig[11]. Much work has gone into examining the correct form of these fluctuations for lattice Boltzmann since then[12–14]. The remaining difficulties with defining consistent fluctuations for lattice Boltzmann systems also hinder the progress for extended version of the fluctuating lattice Boltzmann method for non-ideal systems [15–19].

In this paper we are trying to get away from the unphysical approach of introducing fluctuations in a continuous system through a Langevin approach, and back to a more natural approach of introducing fluctuations by focusing on the discrete nature of the fluid we are examining. The idea of using a lattice gas as an starting point to derive fluctuating lattice Boltzmann methods was pi-

* thomas.blommel@ndsu.edu

† alexander.wagner@ndsu.edu; www.ndsu.edu/pubweb/~carswagn

oneered by Duenweg [12]. The aim of this paper is to derive a discrete lattice gas version that corresponds to current state of the art lattice Boltzmann methods and which would have (at least in close approximation) these lattice Boltzmann methods as its ensemble average.

This paper is structured as follows: we first introduce the basic lattice Boltzmann method and then use these result to propose a lattice gas method with a Monte Carlo collision operator. We then show how this is practically implemented in one and two dimensions. We then consider the Boltzmann limit of this lattice gas implementation and show that it recovers the lattice Boltzmann method that inspired it in the limit of small velocities and small deviations from local equilibrium. The last section shows that this implementation indeed recovers the fluctuating behavior exactly that we perviously tried to impose on the continuous lattice Boltzmann methods.

II. BASIC LATTICE BOLTZMANN

The lattice Boltzmann algorithm consists of densities f_i that are associated with velocities v_i which are lattice velocities. This means that if x is a lattice position, $x + v_i$ will also be a lattice position. These densities are defined on each lattice point x at discrete times t which are taken to be integer values. They evolve in time according to the lattice Boltzmann equation

$$f_i(x + v_i, t + 1) = f_i(x, t) + \Omega_i \quad (1)$$

where Ω_i is the collision operator. In its BGK form this collision operator can be written as

$$\Omega_i = \sum_j \Lambda_{ij} [f_j^0 - f_i(x, t)] + \xi_i \quad (2)$$

where f_i^0 is the local equilibrium distribution and ξ_i is a noise term. Most lattice Boltzmann methods are conserving mass and momentum, but instead of conserving energy they are coupled to a heat bath. We define the local density ρ and momentum density ρu through the velocity moments of the f_i as

$$\rho = \sum_i f_i, \quad (3)$$

$$\rho u_\alpha = \sum_i f_i v_{i\alpha}. \quad (4)$$

Mass and momentum conservation is ensured by the requirement that the local equilibrium distribution also obey

$$\rho = \sum_i f_i^0, \quad (5)$$

$$\rho u_\alpha = \sum_i f_i^0 v_{i\alpha}. \quad (6)$$

For the recovery of the Navier-Stokes equations we also require higher order moments for the equilibrium distribution. From analogy to the velocity moments of the Maxwell-Boltzmann distribution we demand

$$\sum_i f_i^0 (v_{i\alpha} - u_\alpha)(v_{i\beta} - u_\beta) = \rho \theta \delta_{\alpha\beta} \quad (7)$$

$$\sum_i f_i^0 (v_{i\alpha} - u_\alpha)(v_{i\beta} - u_\beta)(v_{i\gamma} - u_\gamma) = Q_{\alpha\beta\gamma} \quad (8)$$

where $Q_{\alpha\beta\gamma}$ should be zero. Unfortunately for small velocity sets typically used which have $v_{i\alpha}^3 = v_{i\alpha}$ because $v_{i\alpha} \in \{-1, 0, 1\}$ this is not possible [20]. But for the special choice of $\theta = 1/3$ it can be reduced to $\rho u_\alpha u_\beta u_\gamma$, which is assumed to be small for $u \ll 1$ found in lattice Boltzmann simulations. An expansion of the continuous Maxwell Boltzmann distribution to second order in velocities then gives

$$f_i^0(\rho, u) = \rho w_i \left(1 + \frac{v_{i\alpha} u_\alpha}{\theta} + \frac{v_{i\alpha} u_\alpha v_{i\beta} u_\beta}{2\theta^2} - \frac{u_\alpha u_\alpha}{2\theta} \right). \quad (9)$$

The w_i are obtained by matching the discrete velocity moments to the continuous velocity moments of the equilibrium distribution. To recover the continuity and Navier-Stokes equations we require the first four moments. All odd moments are zero and the even moments obey

$$\sum_i w_i = 1 \quad (10)$$

$$\sum_i w_i v_{i\alpha} v_{i\beta} = \theta \delta_{\alpha\beta} \quad (11)$$

$$\sum_i w_i v_{i\alpha} v_{i\beta} v_{i\gamma} v_{i\delta} = \theta (\delta_{\alpha\beta} \delta_{\gamma\delta} + \delta_{\alpha\gamma} \delta_{\beta\delta} + \delta_{\alpha\delta} \delta_{\beta\gamma}) \quad (12)$$

The collision matrix Λ_{ij} is constructed so that the stress moments are relaxed at a rate that determines the viscosity, and other moments can be relaxed at different rates [21, 22], *e.g.* to optimize the stability of the method. In general we can write the moments as

$$M^a = \sum_i m_i^a f_i \quad (13)$$

where the first moment would be related to the density (*i.e.* $m_i^0 \propto 1$), the next moments would be proportional to the momentum (*i.e.* $m_i^\alpha \propto v_{i\alpha}$) and the next moments will be related to the stress tensor. For completeness we require as many moments M^a as we have densities f_i so we can have a one-to-one correspondence between moment and velocity space. It is often useful to require that the square matrix generating the moments be orthogonal with respect to some measure. Particularly for fluctuating applications it is often [10, 13, 23] found to be advantageous to require

$$\sum_i w_i m_i^a m_j^a = \delta_{ij}. \quad (14)$$

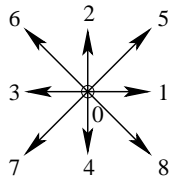


FIG. 1. Numbering scheme for the D2Q9 velocity set.

This implies the backtransform

$$f_i = \sum_a w_i m_i^a M^a \quad (15)$$

as well as

$$\sum_a w_i m_i^a m_i^b = \delta^{ab}. \quad (16)$$

In this representation the collision matrix is designed to be diagonal:

$$\Lambda^{ab} = \sum_{i,j} m_i^a \Lambda_{ij} w_j m_j^b = \frac{1}{\tau^a} \delta^{ab}. \quad (17)$$

Setting the τ^a then fully determines the algorithm. Next we will briefly discuss two common lattice Boltzmann velocity sets for one and two dimensions.

A. D1Q3

The minimal lattice Boltzmann method in one dimension consists of only three velocities corresponding to particle moving to a lattice site to the right, the lattice site to the left or a particle remaining at its lattice site. This is referred to as the D1Q3 model. Our velocity set is given by

$$v_{ix} \in \{-1, 0, 1\}. \quad (18)$$

The weights are given by

$$\begin{aligned} w_0 &= 2/3 \\ w_{-1} &= w_1 = 1/6 \end{aligned} \quad (19)$$

The moment matrix is given by

$$M = \begin{pmatrix} 1 & 1 & 1 \\ -\sqrt{3} & 0 & \sqrt{3} \\ 2\sqrt{\frac{3}{2}} & -\sqrt{\frac{3}{2}} & 2\sqrt{\frac{3}{2}} \end{pmatrix} \quad (20)$$

The first two rows correspond to the conserved mass and momentum moments respectively. So there is only one relaxation time for the moment related to the third row for the D1Q3 model.

B. D2Q9

In the D2Q9 implementation, our velocity set consists of 9 velocities given by the product set of the D1Q3 velocities of Eq. (18):

$$v_i = \begin{bmatrix} v_x \\ v_y \end{bmatrix} \quad (21)$$

where $v_x, v_y \in \{-1, 0, 1\}$. For the D2Q9 model we can define a numbering for the velocities shown in Fig. 1. For the weights we get

$$w_0 = 4/9, \quad (22)$$

$$w_{1-4} = 1/9, \quad (23)$$

$$w_{5-8} = 1/36. \quad (24)$$

The moment matrix is given by

$$M = \begin{pmatrix} 1 & 1 & 1 & 1 & 1 & 1 & 1 & 1 & 1 \\ 0 & \sqrt{3} & 0 & -\sqrt{3} & 0 & \sqrt{3} & -\sqrt{3} & -\sqrt{3} & \sqrt{3} \\ 0 & 0 & \sqrt{3} & 0 & -\sqrt{3} & \sqrt{3} & \sqrt{3} & -\sqrt{3} & -\sqrt{3} \\ 0 & \frac{3}{2} & -\frac{3}{2} & \frac{3}{2} & -\frac{3}{2} & 0 & 0 & 0 & 0 \\ 0 & 0 & 0 & 0 & 0 & 3 & -3 & 3 & -3 \\ -1 & \frac{1}{2} & \frac{1}{2} & \frac{1}{2} & \frac{1}{2} & 2 & 2 & 2 & 2 \\ 0 & -\sqrt{\frac{3}{2}} & 0 & \sqrt{\frac{3}{2}} & 0 & \sqrt{6} & -\sqrt{6} & -\sqrt{6} & \sqrt{6} \\ 0 & 0 & -\sqrt{\frac{3}{2}} & 0 & \sqrt{\frac{3}{2}} & \sqrt{6} & \sqrt{6} & -\sqrt{6} & -\sqrt{6} \\ \frac{1}{2} & -1 & -1 & -1 & -1 & 2 & 2 & 2 & 2 \end{pmatrix} \quad (25)$$

where the numbering of the rows and columns is given by the numbering of the velocities in Figure 1. We then get the moments

$$Mf = \begin{pmatrix} \rho \\ j_x \\ j_y \\ \sigma_- \\ \sigma_{xy} \\ \sigma_+ \\ q_x \\ q_y \\ t \end{pmatrix} \quad (26)$$

This concludes our very brief recap of the lattice Boltzmann algorithm (in its most common form) and we will next present the Monte Carlo lattice Gas algorithm introduced in this paper.

III. THE MONTE CARLO LATTICE GAS ALGORITHM

The main idea behind defining a lattice gas that behaves equivalently to a lattice Boltzmann method is that we will use a Monte Carlo collision operator that explicitly conserves mass and momentum and will recover the correct equilibrium distribution for $u = 0$. For zero

velocity the lattice Boltzmann equilibrium distribution (9) is given simply by

$$f_i^{eq}(\rho, u \equiv 0) = \rho w_i. \quad (27)$$

Let us now consider a collision of two particles with velocities v_i and v_j . We denote the probability of colliding these two particles and ending up with two particles with velocities v_k and v_l with $P_{ij \rightarrow kl}$. We can assume detailed balance, which means that the forward and backward collisions times the probabilities of finding these pairs in equilibrium have to be equal. Let us assume that the number of particles at a lattice site is N . At one lattice site the probability of picking a particle with velocity v_i is then Nw_i . (Strictly speaking the probabilities of picking a second particle are slightly altered by already having picked a particle, a small subtlety that we will neglect for now.) We can then write the detailed-balance condition for the equal probability for the forward and backward collisions as

$$w_i w_j P_{ij \rightarrow kl} = w_k w_l P_{kl \rightarrow ij}. \quad (28)$$

This fixes the ratios of the forward and backward collisions to

$$\frac{P_{ij \rightarrow kl}}{P_{kl \rightarrow ij}} = \frac{w_k w_l}{w_i w_j}. \quad (29)$$

Assuming that we do not have any additional conserved quantities this condition will ensure that the system will approach the lattice Boltzmann equilibrium distribution if the system has a mean velocity of zero. For actual collisions, *i.e.* $ij \neq kl$, we pick the transition probability

$$P_{ij \rightarrow kl} \propto \min\left(1, \frac{w_k w_l}{w_i w_j}\right) \delta_{(v_i+v_j), (v_k+v_l)} \quad (30)$$

where δ is the Kronecker delta. Note that this ensures the probability ratio requirement of Eq. (29), which is always guaranteed for the case $ij = kl$. Next we have to ensure that the probabilities add up to one:

$$\sum_{kl} P_{ij \rightarrow kl} = 1 \quad (31)$$

and of course we also require $P_{ij \rightarrow kl} \geq 0$. Formally we can achieve this by introducing a proportionality factor $\lambda_{ij,kl}$ to get

$$P_{ij \rightarrow kl} = \begin{cases} \lambda_{ij,kl} \min\left(1, \frac{w_k w_l}{w_i w_j}\right) \delta_{(v_i+v_j), (v_k+v_l)} & ij \neq kl \\ 1 - \sum_{kl \neq ij} P_{ij \rightarrow kl} & ij = kl \end{cases} \quad (32)$$

and requiring $\lambda_{ij,kl} = \lambda_{kl,ij}$ to ensure Eq. (29). Note that the lower condition, together with the requirement of positive probabilities, puts an constraint for the largest achievable $\lambda_{ij,kl}$.

The lattice gas algorithm then consists of moving particles according to their associated velocities v_i and then picking C pairs of particles at random and colliding them

according to the transition probabilities given above. We denote the number of particles at position x and time t moving in direction v_i with $n_i(x, t)$. The local density is then given by

$$N(x, t) = \sum_i n_i(x, t). \quad (33)$$

We write the evolution equation as

$$n_i(x + v_i, t + 1) = n_i(x, t) + \Omega_i \quad (34)$$

where the collision operator Ω_i is the effect of M individual collisions on the number of particles moving with velocity v_i . These can be written as picking a pair of particles with velocities v_j and v_k , and then examining the possible outcomes. This gives a random variable ϑ_i that takes on the value

$$\vartheta_i(jklm) = (\delta_{il} + \delta_{im} - \delta_{ij} - \delta_{ik}) \quad (35)$$

with probability $n_j n_k P_{jk \rightarrow lm} / N^2$. And we get the full collision operator as the sum of these random variables:

$$\Omega_i = \sum_{m=1}^M \vartheta_i(jklm). \quad (36)$$

Next we will show two explicit implementations of this algorithm in one and two dimensions for standard velocity sets.

A. A D1Q3 implementation

A state is given by the numbers of particles n_i moving in direction v_i . For this velocity set the only collision that conserves momentum and changes the state of the system consists of two particles moving in opposite directions that come to rest, or the inverse process of two rest particles that will move apart in opposite directions.

$$\{-1, 1\} \rightarrow \{0, 0\} \quad (37)$$

$$\{0, 0\} \rightarrow \{-1, 1\} \quad (38)$$

For the D1Q3 lattice Boltzmann method the weights are given by Eq. (19). We get for the transition probabilities

$$P_{-11 \rightarrow -11} = 1 - \lambda \quad (39)$$

$$P_{-11 \rightarrow -1-1} = 0 \quad (40)$$

$$P_{1-1 \rightarrow 1-1} = 1 - \lambda \quad (41)$$

$$P_{1-1 \rightarrow -11} = 0 \quad (42)$$

$$P_{-11 \rightarrow 00} = \lambda \quad (43)$$

$$P_{1-1 \rightarrow 00} = \lambda \quad (44)$$

$$P_{00 \rightarrow 00} = 1 - \lambda/8 \quad (45)$$

$$P_{00 \rightarrow -11} = \lambda/16 \quad (46)$$

$$P_{00 \rightarrow 1-1} = \lambda/16 \quad (47)$$

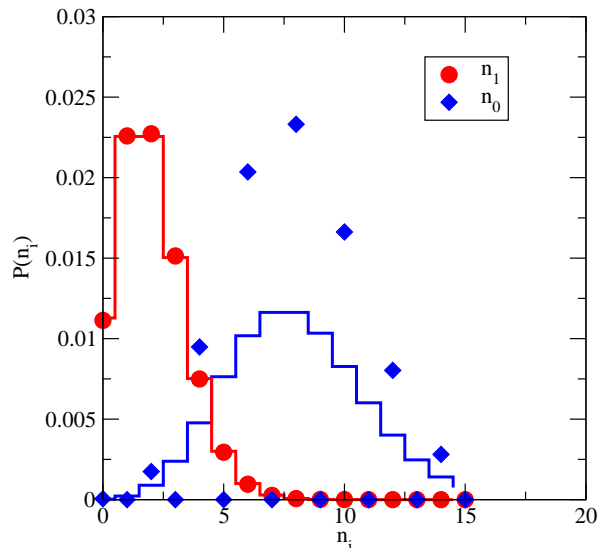


FIG. 2. Poisson-like distributions with additional constraint are found for the D1Q3 model. All lattice sites were initialised with even number of rest particles. $P(n_1) = P(n_{-1})$. Note this conserved quantity does not affect the distribution of moving particles.

where we have set some irrelevant switching probabilities to zero since they do not change the state.

As a consequence of this small collision set, an accidentally conserved quantity is introduced. The number of rest particles at each lattice site will stay either even or odd throughout the entire simulation, as they can only be created or destroyed in pairs. This conserved quantity prevents us from exactly recovering the equilibrium distribution, particularly the Poisson distributions, as shown in Fig. 2

B. A D2Q9 implementation

These velocities of Eq. (21) allow for many more collisions, and these collisions can be grouped into equivalence classes, in which each collision within a class is simply a rotation of the other collisions. In order to ensure isotropy, we must ensure that the $\lambda_{ij,kl}$ for all collisions in an equivalence class are the same.

Some collisions in our D2Q9 model break the conservation of ‘even or odd-ness’ of n_0 at each lattice site. However, in the projection of our simulation along the x or y direction, we still have that each row and column is constant in its ‘even or odd-ness’. This has a much smaller impact on the simulation as our lattice size grows. Let us assume the lattice has L_x lattice sites in the x-direction and L_y lattice sites in the y-direction. Then the number of conserved quantities grows only as $L_x + L_y$, but the number of lattice sites grows as $L_x L_y$, so the fraction of spuriously conserved degrees of freedom becomes small for large lattices.

The equivalence classes are shown schematically in Fig.

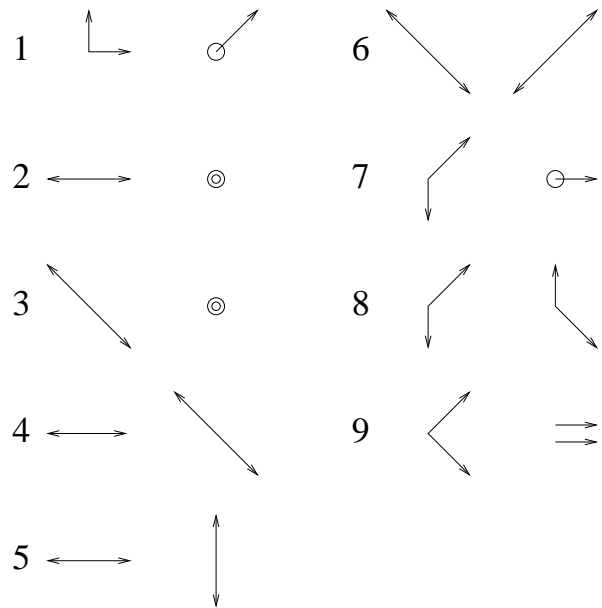


FIG. 3. The 9 equivalence classes for binary collisions that both change the state and conserve momentum. The numbers are used to identify the relaxation rates λ_i corresponding to each equivalence class. Rotated versions of these collisions are implied. Arrows correspond to particles moving with the corresponding velocity v_i , circles denote rest-particles. Each of these collision equivalence classes is associated with a different rate constant $\lambda_{ij,kl}$.

3. This allows us to write down all possible binary collisions and their probabilities in principle, exactly in the same way as we did for the D1Q3 model. We make the simplification that the relaxation rates $\lambda_{ij,kl}$ are instead referred to as λ_i , where each index i refers to the number of the equivalence class identified in Fig. 3. We now have many more collisions, which we will not explicitly list here. It should also be noted that there are three and more particle collisions that could be included. For simplicity those are neglected here.

IV. BOLTZMANN AVERAGE OF THE LATTICE GAS

To compare the lattice gas results to the lattice Boltzmann methods we will now examine an ensemble average of the lattice gas evolution equation. We define the particle densities as

$$f_i(x, t) = \langle n_i(x, t) \rangle \quad (48)$$

where $\langle \rangle$ implies a non-equilibrium average over an ensemble of microscopic realizations leading to the same macroscopic state. We define the density as

$$\rho(x, t) = \langle N(x, t) \rangle. \quad (49)$$

The evolution equation for the average particle densities is then

$$f_i(x + v_i, t + 1) = f_i(x, t) + \Xi_i \quad (50)$$

where we have defined the averaged collision operator

$$\Xi_i = \sum_{jklm} \vartheta_i(jklm) \frac{f_j f_k}{\rho^2} P_{jk \rightarrow lm}. \quad (51)$$

From this collision operator we can obtain the equilibrium distributions for the f_i by demanding

$$0 = \sum_{jklm} \vartheta_i(jklm) \frac{f_j^{eq} f_k^{eq}}{\rho^2} P_{jk \rightarrow lm}. \quad (52)$$

This gives us a quadratic matrix equation in the equilibrium density. One might expect not to obtain a unique solution. However, since we require that $f_i^{eq} > 0$ we will find below that only one physical solution survives.

A. D1Q3 results

In the one-dimensional case of D1Q3 we find that Eq. (51) gives

$$\Xi(\{f_i\}) = \frac{\lambda}{\rho^2} \begin{bmatrix} \frac{f_0^2}{8} - 2f_{-1}f_1 \\ 4f_{-1}f_1 - \frac{f_0^2}{4} \\ \frac{f_0^2}{8} - 2f_{-1}f_1 \end{bmatrix}. \quad (53)$$

The equilibrium distribution has to be found with respect to the corresponding conserved quantities of mass $N(x, t)$ and the momentum

$$N(x, t)U(x, t) = \sum_i n_i(x, t)v_i. \quad (54)$$

This corresponds to an ensemble averaged momentum of

$$\rho(x, t)u(x, t) = \langle N(x, t)U(x, t) \rangle. \quad (55)$$

We can use a matrix that transforms the f_i vector onto the conserved moments and one free moment of Eq. (20).

We then have the moments

$$M \begin{bmatrix} f_{-1} \\ f_0 \\ f_1 \end{bmatrix} = \begin{bmatrix} \rho \\ \sqrt{3}\rho u \\ \pi \end{bmatrix}. \quad (56)$$

We can then write the collision operator in this moment space as

$$\begin{aligned} M\Xi(f_i) &= \frac{\lambda}{\rho^2} \begin{bmatrix} 0 \\ 0 \\ \sqrt{\frac{27}{32}}(f_0^2 - 16f_{-1}f_1) \end{bmatrix} \\ &= \frac{\lambda}{\rho^2} \begin{bmatrix} 0 \\ 0 \\ \frac{18u^2\rho^2 - \pi(\pi + \sqrt{24}\rho)}{\sqrt{24}} \end{bmatrix}. \end{aligned} \quad (57)$$

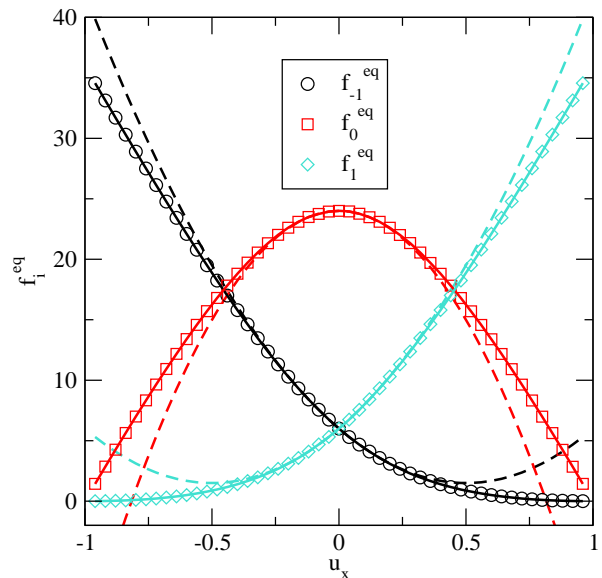


FIG. 4. Comparison between the measured average $\langle n_i \rangle$ (shown as symbols) and the predicted equilibrium distribution, f_i^{eq} , of Eq. (60) (shown as solid lines) for the D1Q3 model. This is also compared to the lattice Boltzmann equilibrium distribution, f_i^0 , of Eq. (9).

In equilibrium the collision operator does not change the distributions. Reversely, we can find the equilibrium distribution by demanding that the collision operator be zero. Thus we obtain π^{eq} in terms of the conserved quantities as

$$\pi^{eq} = \sqrt{6}\rho(-1 \pm \sqrt{1 + 3u^2}). \quad (58)$$

The solution with the negative sign leads to negative densities, while the other solution stays positive. We obtain the D1Q3 equilibrium distribution

$$\begin{bmatrix} f_{-1}^{eq} \\ f_0^{eq} \\ f_1^{eq} \end{bmatrix} = \begin{bmatrix} \frac{\rho}{6}(-1 - 3u + 2\sqrt{1 + 3u^2}) \\ \frac{2\rho}{3}(2 - \sqrt{1 + 3u^2}) \\ \frac{\rho}{6}(-1 + 3u + 2\sqrt{1 + 3u^2}) \end{bmatrix} \quad (59)$$

which can be written as

$$\begin{aligned} f_i^{eq}(\rho, u_x) \\ = \rho w_{v_{ix}} \left[1 + 3v_{ix}u_x + (3v_{ix}^2 - 1)(\sqrt{1 + 3u_x^2} - 1) \right]. \end{aligned} \quad (60)$$

We show a comparison of a measured equilibrium distribution to this prediction in Fig. 4. For the measured equilibrium distribution we show results for $\langle N \rangle = 36$, $\lambda = 1$, a lattice size of $L_x = 100$. We used $C = 10$ collisions per iteration step and the simulation was initially run for 15,000 steps to equilibrate the simulation, and then another 15,000 iterations were used for the measurements. We find excellent agreement between this prediction and our measurements of the equilibrium distribution. The agreement between our new equilibrium

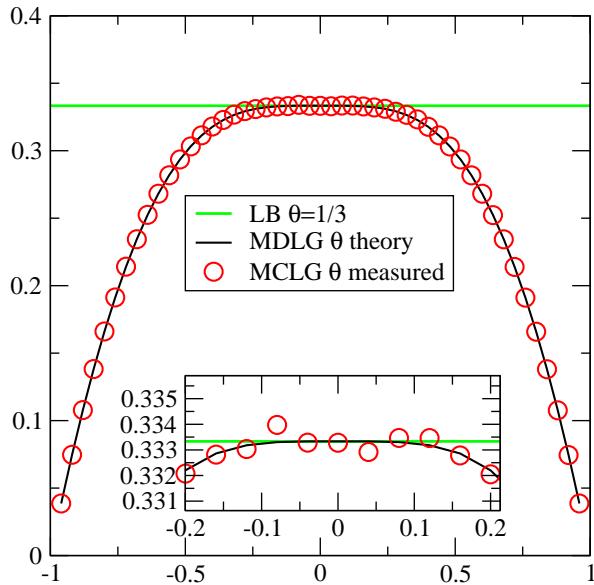


FIG. 5. Second velocity moment of Eq. (7) divided by the mean density for the MCLG equilibrium distribution for D1Q3. The crucial result here is that in the relevant region $|u| < 0.1$ there is excellent agreement between the standard LB result and the MCLG result.

distribution and that of a standard LB equilibrium distribution function of Eq. (9) is also close for $|u| < 0.4$, but diverges thereafter.

This difference implies that the second moment of the equilibrium distribution will not obey the lattice Boltzmann requirement of Eq. (7) for all u . This is not surprising since the MCLG equilibrium distribution, unlike its LB equivalent, is positive definite. This means that for a velocity of $u = \pm 1$ we require $f_{\pm 1} = \rho$, and therefore the second moment must be zero for this extreme value. However lattice Boltzmann simulations typically require $u \ll 1$, which is usually taken as $u < 0.1$, so disagreements between these equilibrium distributions outside the range $|u| < 0.1$ have little practical relevance.

We show the second moment of Eq. (7) for our MDLG equilibrium distribution in Fig. 5. As predicted, the effective temperature for the MCLG method goes to zero for large absolute velocities, as is unavoidable for a discrete method with a restricted velocity set that has positive definite occupation numbers. For the relevant region where $|u| < 0.1$, however there is excellent agreement between the MCLG and LB results, as shown in the inset.

After identifying the equilibrium distribution for the D1Q3 MCLG, we should now examine the collision operator more closely. Eq. (57) implies that the collision operator leaves the mass and momentum modes unchanged (as it has to, since those are conserved) and only alters the π mode. Let us define its deviation from equilibrium as $\tilde{\pi} = \pi - \pi^{eq}$. If we denote $\tilde{\pi}_{(k)}$ as the value of $\tilde{\pi}$ after

k collisions we can write the effect of one collision as

$$\tilde{\pi}_{(k+1)} = \tilde{\pi}_{(k)} - \frac{\lambda}{2\sqrt{6}} \left(\frac{\tilde{\pi}_{(k)}^2}{\rho^2} + \frac{\tilde{\pi}_{(k)}}{\rho} 2\sqrt{6}\sqrt{1+3u^2} \right). \quad (61)$$

If we interpret this as a differential equation we can write the analytical solution as

$$\tilde{\pi}_{(k)} = \frac{2\sqrt{6}\rho\sqrt{1+3u^2}\tilde{\pi}_{(0)}}{\exp\left(\frac{k\lambda\sqrt{1+3u^2}}{\rho}\right)(2\sqrt{6}\rho\sqrt{1+3u^2} + \tilde{\pi}_{(0)}) - \tilde{\pi}_{(0)}}. \quad (62)$$

For the standard BGK approach in lattice Boltzmann we would have expected a pure exponential decay, corresponding to the approximation of neglecting $\tilde{\pi}^2$ in Eq. (61). The connection between the LG collision operator and the LB BGK collision operator is interesting. The collision MCLG operator is quadratic (and would also involve higher powers if we allowed for multi-particle collisions), but the BGK operator is linear. This apparent mismatch is resolved by writing the collision operator in terms of the moments, and examine only the decay of the deviatoric moments. In such a representation close to local equilibrium all moments are small, except for the conserved moments, most notably the density. So quadratic terms that connect a mode to the local density will dominate the collision operator, and since the density does not change during the collision, the linear relaxation of those moments is recovered. Explicitly we have for small $\tilde{\pi}$

$$\Lambda^{ab} = \begin{pmatrix} 0 & 0 & 0 \\ 0 & 0 & 0 \\ 0 & 0 & 1/\tau^\pi \end{pmatrix} \quad (63)$$

where

$$\tau^\pi = \frac{\tilde{\pi}_{(0)}}{\tilde{\pi}_{(0)} - \tilde{\pi}_{(M)}}. \quad (64)$$

In principle this is now a state dependent relaxation rate, but for small $\tilde{\pi}_M$ we get

$$\tau^\pi \approx \frac{1}{1 - \exp\left(-\frac{M\lambda\sqrt{1+3u^2}}{\rho}\right)}. \quad (65)$$

This means that the range of reachable relaxation times are given by $\tau^\pi \in [1, \infty]$. For simple collisions the important over-relaxation regime for $\tau \in [1/2, 1]$ that is often utilized in lattice Boltzmann simulations is unavailable for this lattice gas method.

We test our analytical prediction of the decay of the π mode by averaging over 1000 realizations of an initial configuration of $n_i(x, 0) = \{100, 100, 100\}$ on a system with $L_x = 1000$ and $\lambda = 1$ and examine the decay of $\langle \pi \rangle$ as a function of the number of collisions. Interestingly we have to consider the average relaxation of π in a full simulation, including streaming, since our prediction of the equilibrium distribution allowed us to obtain the

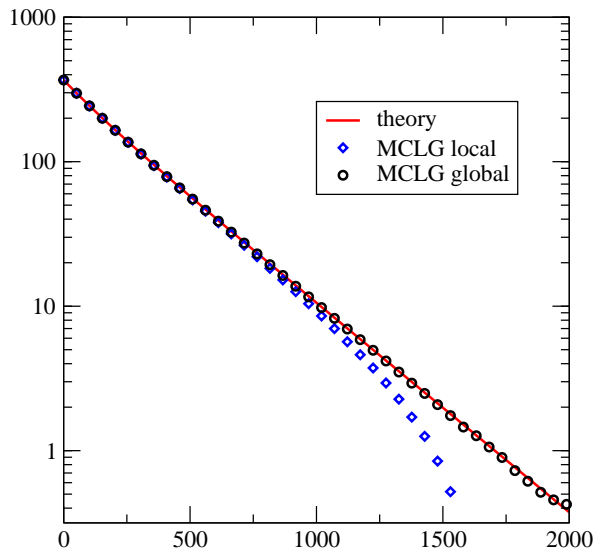


FIG. 6. Measured and theoretical decay of the second moment of a D1Q3 simulation. We observe excellent agreement between the simulation and prediction of Eq. (62) for the relaxation of $\tilde{\pi}_{(k)}$ as a function of k towards global equilibrium. Also shown is the relaxation towards local equilibrium for a simulation without streaming, which will lead to a negative $\tilde{\pi}$ because the second moment of the local distribution has a smaller value.

global equilibrium distribution, not the local equilibrium distribution. The π moment for a simulation without streaming, which only allows for local collisions, will be less than the equilibrium moment, because velocity fluctuations contribute to the second moment of the global equilibrium distribution. These results are shown in Figure 6. Note that without fluctuations the difference between global and local equilibrium distributions would disappear here.

B. D2Q9 results

The derivation of the D2Q9 collision operator follows the D1Q3 derivation we just showed, but because we have 6 modes that relax, instead of just 1, collision rules become too lengthy to write down. They are easily derived from the collision classes presented in Figure 3. We now have nine λ_i which make the equivalent of Eq. (53) again too lengthy to write down. The equivalent of Eq. (57) shows a similar structure: many quadratic terms in the m_i . Of the $9^3 = 729$ possible combinations 243 actually occur, each typically associated with several λ_i , again making this too much too large to display in a paper. However, if we neglect all combinations of moments other than the moments related to the mass, which is the largest moment, we obtain

$$M\Xi = 2 \begin{bmatrix} 0 \\ 0 \\ 0 \\ \rho\sigma_- \left(-\frac{2}{9}\lambda_2 - \frac{1}{36}\lambda_4 - \frac{4}{9}\lambda_5 - \frac{2}{9}\lambda_7 - \frac{1}{36}\lambda_9 \right) \\ \rho\sigma_{xy} \left(-\frac{4}{9}\lambda_1 - \frac{1}{18}\lambda_3 - \frac{1}{9}\lambda_4 - \frac{1}{9}\lambda_6 - \frac{2}{9}\lambda_7 - \frac{4}{9}\lambda_8 \right) \\ -\frac{2}{9}\rho \left((\sigma_+ - t)\lambda_2 + \left(\frac{1}{4}\sigma_+ + \frac{1}{8}t\right)\lambda_3 + \left(\frac{1}{8}\sigma_+ + \frac{1}{4}t\right)\lambda_4 + \left(\sigma_+ + \frac{1}{2}t\right)\lambda_7 + \left(\frac{1}{8}\sigma_+ + \frac{1}{4}t\right)\lambda_9 \right) \\ \rho q_x \left(-\frac{2}{3}\lambda_1 - \frac{1}{3}\lambda_7 - \frac{1}{3}\lambda_8 - \frac{1}{12}\lambda_9 \right) \\ \rho q_y \left(-\frac{2}{3}\lambda_1 - \frac{1}{3}\lambda_7 - \frac{1}{3}\lambda_8 - \frac{1}{12}\lambda_9 \right) \\ -\rho \left(t\lambda_1 + \left(\frac{2}{9}t - \frac{2}{9}\sigma_+\right)\lambda_2 + \left(\frac{1}{36}\sigma_+ + \frac{1}{72}t\right)\lambda_3 + \left(\frac{1}{18}\sigma_+ + \frac{1}{9}t\right)\lambda_4 + \left(\frac{1}{9}\sigma_+ + \frac{1}{18}t\right)\lambda_7 + \left(\frac{1}{18}\sigma_+ + \frac{1}{9}t\right)\lambda_9 \right) \end{bmatrix} \quad (66)$$

We see that the relaxation of all moments decouples, except for the σ_+ and t moments. To recover a diagonal collision matrix in moment space is equivalent to decoupling here. The 8th moment couples to σ_+ with a the same coefficient that the 5th moment couples to the eighths. We can set this coefficient to zero by demanding:

$$\frac{2}{9}\lambda_2 - \frac{1}{36}\lambda_3 - \frac{1}{18}\lambda_4 - \frac{1}{9}\lambda_7 - \frac{1}{18}\lambda_9 = 0 \quad (67)$$

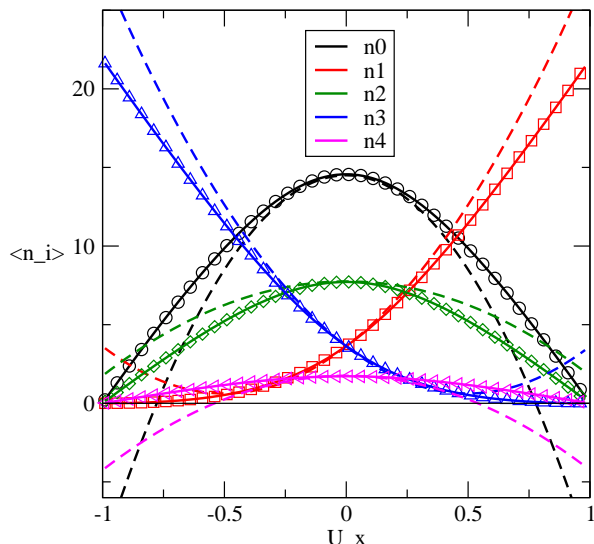
which then decouples the modes and recovers the diagonal collision matrix for D2Q9. Additionally, for the isotropy of the stress tensor, we demand that the σ_{xy}

and σ_- be relaxed at the same rate:

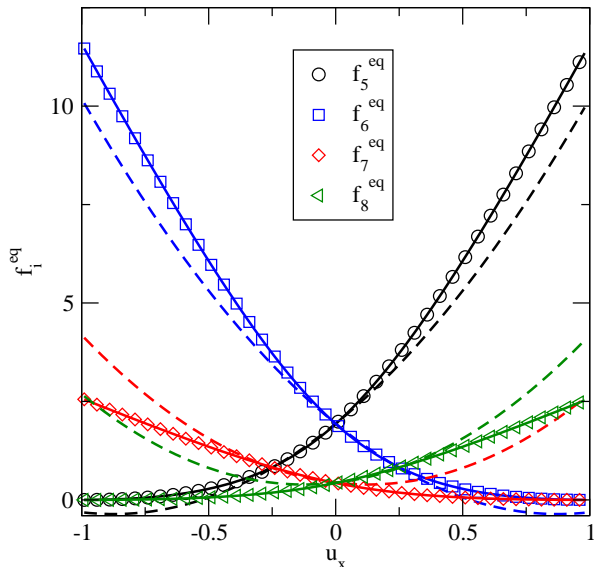
$$\begin{aligned} & \left(-\frac{2}{9}\lambda_2 - \frac{1}{36}\lambda_4 - \frac{4}{9}\lambda_5 - \frac{1}{36}\lambda_9 \right) \\ & = \left(-\frac{4}{9}\lambda_1 - \frac{1}{18}\lambda_3 - \frac{1}{9}\lambda_4 - \frac{1}{9}\lambda_6 - \frac{4}{9}\lambda_8 \right). \end{aligned} \quad (68)$$

The moments q_x and q_y are already relaxed at the same rate.

This means we have derived a multi-relaxation-time BGK collision operator (with the assumption that we are close enough to equilibrium that the density mode is much larger than the non-conserved moments) from the underlying lattice gas collision rules. We believe that this is the first such derivation. All earlier introductions of a BGK collision operator did so as an ad-hoc assumption.



(a)



(b)

FIG. 7. Comparison of measured equilibrium distribution for the lattice gas, the theoretical prediction of Eq. (69), shown as solid lines, and the lattice Boltzmann equilibrium distribution of Eq. (9), shown as dotted lines. We show the results as a function of u_x and have set $u_y = 0.25$ to visually separate the different averages. For smaller u_y the agreement between MCLG and LB results increases.

To calculate the equilibrium distribution we need to set $\Xi^a = 0$. This initially appeared like a hard problem, and Mathematica was unable to solve the resulting equations. However, we noticed that using the product of two one-

dimensional equilibrium distribution functions

$$f_i^{eq}(\rho, u) = \rho \prod_{\alpha} w_{v_{i\alpha}} \left[1 + 3v_{i\alpha}u_{\alpha} + (3v_{i\alpha}^2 - 1)(\sqrt{1 + 3u_{\alpha}^2} - 1) \right] \quad (69)$$

turns out to be the simple solution (no summations over repeated Greek indices is implied here).

Because the w_i are found with an implied mean velocity of zero, when the mean velocity is non-zero, there is no a priori reason for the lattice Boltzmann and MDLG results to agree in this regime. We examine the agreement between the MDLG and the LG results. To do so we used a lattice with dimensions $L_x = 100$, $L_y = 10$, $C = 10$, $\lambda_1 = 15/128$, $\lambda_{2-7} = 1/4$, $\lambda_8 = 1/8$, $\lambda_9 = 18/144$, $\langle \rho \rangle = 36$ and $\langle NU_y \rangle = 0.25$. We varied $\langle NU_x \rangle$. We then iterated over 20,000 iterations to ensure we are in equilibrium and then measured for another 10,000 iterations. The results of these simulations are shown in Fig. 7. As expected our values for the f_i^{eq} agree exactly with the measured values for the lie exactly on top of the predicted values for the Lattice Boltzmann theory around $u_x^{eq} = 0$. At this point, the two models begin to diverge. This is expected because as the mean velocity begins to rise in Lattice Boltzmann simulations, the n_i go negative, which is an unphysical result. Fig. 7 shows that the equilibrium given in Eq. (69) indeed agrees closely with our simulation results.

V. FLUCTUATING PROPERTIES OF THE MCLG

So far we have focused on the Boltzmann average of our lattice gas. The original reason we were interested in the lattice gas were its fluctuating properties. One key assumption that is made in developing fluctuating lattice Boltzmann methods is that for an ideal gas the densities should obey a Poisson statistic. In the lattice Boltzmann context this is problematic, since the densities f_i are continuous, and there is no generally accepted extension of the Poisson statistic to continuous variables. Nonetheless this can be approximately true, as seen in recent papers by Kaehler et al. [13] as well as by Wagner et al. [14]. However, these solutions are never exact and it is important to be aware of where the assumption of Poisson distributed f_i , which is used as an input to derive these methods, breaks down in the practical implementation.

We can formally write the assumption of independently Poisson distributed occupation numbers as

$$P(n_i) = \frac{\exp(-f_i^{eq})(f_i^{eq})^{n_i}}{n_i!}. \quad (70)$$

As a consequence we obtain

$$\langle n_i(x, t)n_j(y, t) \rangle = f_i^{eq}f_j^{eq} + f_i^{eq}\delta_{ij}\delta_{xy} \quad (71)$$

	0	1	2	3	4	5	6	7	8
0	0.998863	-0.000028	-0.000482	-0.000170	-0.000343	0.000001	-0.000114	-0.000082	0.000010
1	-0.000028	0.999171	0.000001	0.000143	-0.000072	-0.000127	-0.000047	0.000013	0.000057
2	-0.000482	0.000001	0.999809	-0.000112	0.000177	-0.000515	-0.000110	-0.000022	0.000482
3	-0.000170	0.000143	-0.000112	1.000230	-0.000079	0.000014	0.000008	-0.000048	-0.000067
4	-0.000343	-0.000072	0.000177	-0.000079	0.999648	0.000492	-0.000023	-0.000103	-0.000480
5	0.000001	-0.000127	-0.000515	0.000014	0.000492	-0.999567	-0.000065	-0.000046	0.000593
6	-0.000114	-0.000047	-0.000110	0.000008	-0.000023	-0.000065	0.999801	-0.000085	0.000086
7	-0.000082	0.000013	-0.000022	-0.000048	-0.000103	-0.000046	-0.000022	0.999687	-0.000117
8	0.000010	0.000057	0.000482	-0.000067	-0.000480	0.000593	0.000086	-0.000117	0.999215

TABLE I. Representation of the correlator of Eq. (72) for the worst statistical outlier for $u_x = -0.68$ of Figure 9.

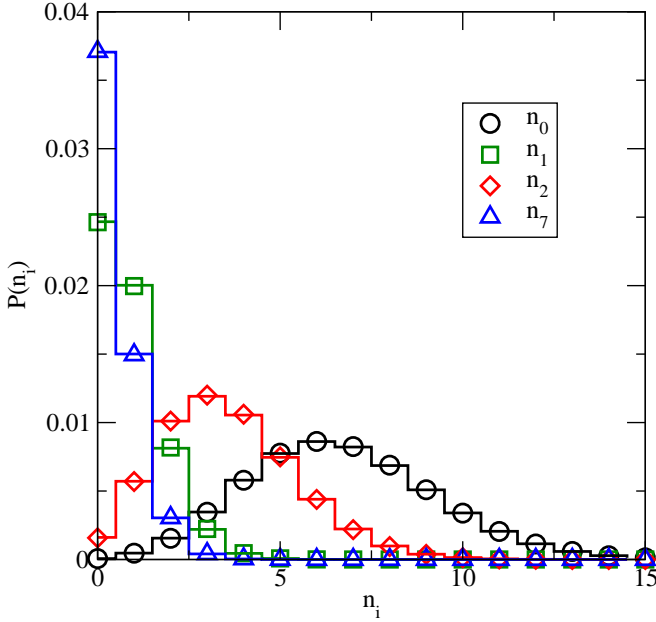


FIG. 8. n_0, n_1, n_2, n_7 , plotted with respect to local density at $U_x = -0.25, U_y = 0.25$ and $\rho = 18$. Symbols represent the measured values while the solid lines are the theoretical distribution.

which is often used as a starting point for the derivation of fluctuating lattice Boltzmann methods.

We tested the prediction of Poisson distributed occupation numbers n_i for a large variety of densities and imposed velocities and throughout found excellent agreement with the prediction from Eq. (70). An example is shown in Figure 8. Similarly we can test the independence of the n_i by looking at

$$\frac{\langle n_i n_j \rangle - f_i^{eq} f_j^{eq}}{\sqrt{f_i^{eq} f_j^{eq}}} \stackrel{?}{=} \delta_{ij}. \quad (72)$$

Again we found excellent agreement for all densities and velocities that we tested. We used the same values for λ_i as above, we initialized the lattice with a density of 360 and an initial velocity u_x with $u_y = 0$. We performed $C = 10$ collisions per iteration. We then discarded the

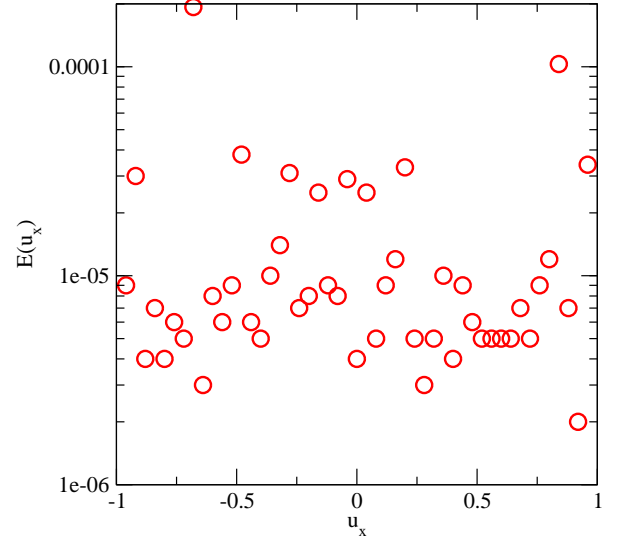


FIG. 9. The deviation of the expected Poisson distribution statistic from the measured correlations from Eq. (73) for different velocities u . There is no discernible pattern, and the error continues to decrease with increased averaging.

first 150,000 iterations to ensure we are looking at an equilibrium systems. We averaged over the next 500,000 steps on a lattice with $L_x = 100, L_y = 10$. We show the worst case result in Table I. We see that we have excellent agreement with our prediction of Eq. (72).

To examine the prediction for different velocities without printing many of these tables we look at a measure of the deviation of the correlation matrix from the expected value

$$E(u_x, u_y) = \sum_{i,j} \left(\frac{\langle n_i n_j \rangle - f_i^{eq} f_j^{eq}}{\sqrt{f_i^{eq} f_j^{eq}}} - \delta_{ij} \right)^2. \quad (73)$$

A graph of this error function as a function of the velocity is shown in Figure 9. We see that there is no apparent systematic variation of this error function with u even for extreme values for u and with increasing averaging the error continues to diminish. This suggests that we have found a reference lattice gas implementation that exactly

fulfills the predictions for a fluctuating ideal gas.

VI. CONCLUSIONS

In this article we have introduced a lattice gas method which employs a Monte Carlo collision operator. We show that the Boltzmann limit of this lattice gas recovers the usual lattice Boltzmann method for moderate velocities $|u| < 0.1$. Remarkably we were able to derive a BGK collision operator from first principles here. Previous the BGK collision operator had been postulated only, but not derived. The equilibrium distribution has interesting properties, reminiscent of other recently proposed equilibrium distributions in the context of entropic lattice Boltzmann [24] and cascading lattice Boltzmann

[25]. Presumably this method will obey an H-theorem, but we have not as yet identified the corresponding H-functional.

Remarkably the fluctuating properties of this MCLG recover Poisson statistics exactly, even outside the range where the MCLG approach agrees with common lattice Boltzmann methods. This suggests that an optimized version of this MCLG method may become a promising contender for the simulation of fluctuating fluids. However, developing an implementation that can compete with lattice Boltzmann approaches on speed will require a very clever implementation of a lattice gas collision operator that can perform multiple collisions at one time and a way to introducing over-relaxation that has been the way of lowering transport coefficients below the value obtained for full relaxation to local equilibrium.

-
- [1] A. Einstein, *Annalen der physik* **324**, 371 (1906).
 - [2] K. Kawasaki, *Annals of Physics* **61**, 1 (1970).
 - [3] D. S. Lemons and A. Gythiel, *American Journal of Physics* **65**, 1079 (1997), <http://dx.doi.org/10.1119/1.18725>.
 - [4] U. Frisch, B. Hasslacher, and Y. Pomeau, *Physical review letters* **56**, 1505 (1986).
 - [5] U. Frisch, D. dHumieres, B. Hasslacher, P. Lallemand, Y. Pomeau, J.-P. Rivet, *et al.*, *Complex systems* **1**, 649 (1987).
 - [6] G. R. McNamara and G. Zanetti, *Physical review letters* **61**, 2332 (1988).
 - [7] F. J. Higuera, S. Succi, and R. Benzi, *EPL (Europhysics Letters)* **9**, 345 (1989).
 - [8] A. J. Ladd, M. E. Colvin, and D. Frenkel, *Physical review letters* **60**, 975 (1988).
 - [9] A. J. Ladd, *Physical Review Letters* **70**, 1339 (1993).
 - [10] R. Adhikari, K. Stratford, M. Cates, and A. Wagner, *EPL (Europhysics Letters)* **71**, 473 (2005).
 - [11] M. Bixon and R. Zwanzig, *Physical Review* **187**, 267 (1969).
 - [12] B. Dünweg, U. D. Schiller, and A. J. Ladd, *Physical Review E* **76**, 036704 (2007).
 - [13] G. Kaehler and A. Wagner, *Physical Review E* **87**, 063310 (2013).
 - [14] A. J. Wagner and K. Strand, *Physical Review E* **94**, 033302 (2016).
 - [15] M. Gross, R. Adhikari, M. Cates, and F. Varnik, *Physical Review E* **82**, 056714 (2010).
 - [16] S. T. Ollila, C. Denniston, M. Karttunen, and T. AlaNissila, *The Journal of chemical physics* **134**, 064902 (2011).
 - [17] S. P. Thampi, I. Pagonabarraga, and R. Adhikari, *Physical Review E* **84**, 046709 (2011).
 - [18] M. Gross and F. Varnik, *Physical Review E* **85**, 056707 (2012).
 - [19] D. Belardinelli, M. Sbragaglia, L. Biferale, M. Gross, and F. Varnik, *Physical Review E* **91**, 023313 (2015).
 - [20] A. Wagner and Q. Li, *Physica A: Statistical Mechanics and its Applications* **362**, 105 (2006).
 - [21] D. d'Humieres, *Progress in Astronautics and Aeronautics* **159**, 450 (1994).
 - [22] P. Lallemand and L.-S. Luo, *Physical Review E* **61**, 6546 (2000).
 - [23] G. Kaehler and A. J. Wagner, *Communications in Computational Physics* **13**, 614 (2013).
 - [24] S. S. Chikatamarla, S. Ansumali, and I. V. Karlin, *Phys. Rev. Lett.* **97**, 010201 (2006).
 - [25] M. Geier, A. Greiner, and J. G. Korvink, *Phys. Rev. E* **73**, 066705 (2006).